Phys. Status Solidi RRL **8**, No. 2, 172–175 (2014) / **DOI** 10.1002/pssr.201308238

pss +++rapid research letters+++
www.pss-rapid.com

Ultra-thin (002)-oriented Al-doped zinc oxide transparent electrode grown on oxygen-controlled homo-seed layer

Muqin Wang[1], Ye Yang[,1], Pinjun Lan[1], Ke Zhu[1], Jinhua Huang[1], Yuehui Lu[1], Ruiqin Tan[2], and Weijie Song[*,1]**

[1] Ningbo Institute of Material Technology and Engineering, Chinese Academy of Sciences, Ningbo 315201, P.R. China
[2] Faculty of Information Science and Engineering, Ningbo University, Ningbo 315211, P.R. China

Received 21 October 2013, revised 28 November 2013, accepted 28 November 2013
Published online 4 December 2013

Keywords zinc oxide, films, magnetron sputtering, transparent conducting oxides

[*] Corresponding author: e-mail weijiesong@nimte.ac.cn, Phone/Fax: +86 574 87913375
[**] e-mail yangye@nimte.ac.cn, Phone/Fax: +86 574 87913375

Highly (002)-oriented Al-doped zinc oxide (AZO) thin films with the thickness of less than 200 nm have been deposited on an oxygen-controlled homo-seed layer at 200 °C by DC magnetron sputtering. With the homo-seed layer being employed, the full-width at half maximum (FWHM) of the (002) diffraction peak for the AZO ultra-thin films decreased from 0.33° to 0.22°, and, the corresponding average grain size increased from 26.8 nm to 43.0 nm. The XRD rocking curves revealed that the AZO ultra-thin film grown on the seed layer deposited in atmosphere of O_2/Ar of 0.09 exhibited the most excellent structural order. The AZO ultra-thin film with homo-seed layer reached a resistivity of 4.2×10^{-4} Ω cm, carrier concentration of 5.2×10^{20} cm^{-3} and mobility of 28.8 cm^2 V^{-1} s^{-1}. The average transmittance of the AZO ultra-thin film with homo-seed layer reached 85.4% in the range of 380–780 nm including the substrate.

© 2014 WILEY-VCH Verlag GmbH & Co. KGaA, Weinheim

www.spm.com.cn

1 Introduction Al-doped zinc oxide (AZO), one of the transparent conductive oxides (TCOs), has attracted a great deal of attention due to its many advantages, and has been a promising alternative to indium tin oxide (ITO) for transparent electrodes in flat panel displays (FPDs) [1, 2]. Minami et al. [3] pointed out that the transparent electrodes used in FPDs should have a thickness below 200 nm and a resistivity lower than 5×10^{-4} Ω cm at a substrate temperature below approximately 200 °C. In a conventional sputtering process at a substrate temperature (T_s) of 200 °C, the typical film resistivity is ~6–8 × 10^{-4} Ω cm with a thickness of 200–700 nm [4, 5]. It has been proven that the hydrogenation of aluminum doped zinc oxide (HAZO) film during sputtering may help to improve the properties at low T_s [6–9]. Nevertheless, as far as polycrystalline ZnO-based films are concerned, the electrical property deteriorates rapidly with the decrease of thickness, especially down to 200 nm, which is due to the poor crystalline quality for ultra-thin film [10, 11] causing a severe scattering occurring at crystallographic defects [12], ionized impurities, grain barriers, grain boundaries [13, 14] and the structural disorder [15, 16]. Birkholz et al. [16] emphasized that the perfect preferred orientation order of ZnO crystallites, i.e. (002) texture, was one of the key parameters for the preparation of films with optimized properties. Hence, it is still a challenge to fabricate ultra-thin AZO films by controlling the growth of the initial layer for promoting the structural order of the following film. In order to reach these aims, different deposition methods, such as pulsed laser deposition (PLD) [17], ion beam assisted deposition (IBAD) [18, 19], ion plating with DC arc discharge [20, 21], and the introduction of a hetero- [22, 23] or homo-seed layer [24–27] before the growth of the bulk films, have been adopted. Though significant achievements have been made, a simple and scalable sputtering process for preparing AZO ultra-thin films still needs further development. In this regard, 180 nm AZO ultra-thin films grown on a 10 nm oxygen-controlled homo-seed layer were fabricated by DC magnetron sputtering and exhibited excellent properties. Two layers were grown continuously using the same target at 200 °C without breaking vacuum. The effects of the oxygen-controlled homo-seed layer on

© 2014 WILEY-VCH Verlag GmbH & Co. KGaA, Weinheim

the structural, electrical and optical properties have been investigated.

2 Experimental The AZO ultra-thin films grown on an oxygen-controlled homo-seed layer were deposited on low-iron glass ($100 \times 100 \times 3.2$ mm^3) using direct-current (DC) magnetron sputtering. The target was a homemade 3-inch ceramic disk consisting of 98 wt% ZnO and 2 wt% Al_2O_3 [28]. In the DC magnetron sputtering, the base pressure was 4.0×10^{-4} Pa, and the deposition temperature was kept at 200 °C. The homo-seed layers were firstly deposited at a DC power of 60 W and a pressure of 0.6 Pa with sputtering atmosphere of $O_2/Ar = 0$ and 0.09, named SO_0 and $SO_{0.09}$ samples. The AZO ultra-thin films were then deposited on the SO_0 and $SO_{0.09}$ samples in the sputtering atmosphere of Ar + 8 vol% H_2 at a DC power of 200 W and a pressure of 0.2 Pa using the same target. For comparison, the AZO sample without any seed layer was also prepared in the same sputtering condition and named NS sample.

The thickness of the seed layers was fixed at 10 nm, which was determined by the sputtering rate and time. The thickness of the deposited AZO ultra-thin films was kept at 180 ± 10 nm, which was characterized by a M-2000DI Ellipsometer (J. A. Woollam) according to the Cauchy model. The phase structure of the films was analyzed by X-ray diffraction (XRD) with Cu K_α radiation (Bruker, AXS D8 Advance). The XRD rocking curves were employed in a random direction ($\Phi = 0°$) and perpendicular to it ($\Phi = 90°$) by a high resolution XRD (Bruker AXS D8 Discover). The resistivity, Hall mobility and carrier concentration of the AZO films were analyzed by Hall measurement with the Van der Pauw method (Accent; HL5500PC; UK). The transmittance of the films was measured by a UV–Vis–NIR spectrophotometer (Perkin Elmer Lambda 950). The surface morphologies and roughness were observed over a scan area of 1×1 μm^2 by an atomic force microscope (AFM, CSPM 5500).

3 Results and discussion

3.1 Structural properties Figure 1(a–c) present the XRD curves of NS, SO_0 and $SO_{0.09}$ samples, respectively. Obviously, all the samples reveal the preferred (002) orientation. The intensity of the (002) peak of the AZO ultra-thin films with a homo-seed layer increases markedly, especially for the $SO_{0.09}$ sample. The (002) diffraction peak of the AZO thin films shifts from 34.31° to 34.32° with respect to the reference strain-free ZnO film (34.40°), implying a reduction of residual stress. The full-width at half maximum (FWHM) of the (002) peak of the AZO films decreases from 0.33° to 0.22° with an introduced homo-seed layer. The average grain size calculated according to the Scherrer equation increased from 26.8 nm to 43.0 nm. These results imply an improvement of crystalline quality. Fujimura et al. [29] demonstrated that a proper oxygen diluted argon gas minimizes the ratio of Zn/ZnO in the vapor phase, promoting the formation of ZnO tetrahedral coordination, which has the effect of approaching the deposition state to equilibrium state. In this case, the surface plane of each three-dimensional ZnO nucleus must be (002) plane in the equilibrium deposition state, therefore, an excellent (002)-textured seed layer with nearly perfect crystal nucleus can be obtained by being deposited in the atmosphere of oxygen diluted argon [29]. The second AZO layer will grow along the (002)-oriented seed layer due to the native self-texture properties of ZnO. So the initial seeding layer plays an important role in controlling the orientation and crystallinity of the whole AZO ultra-thin films. To further investigate the improvement of structural order, the rocking XRD scan curves with $\Phi = 0°$ and 90° are presented in Fig. 1(d–f). It is apparent that the AZO ultra-thin films grown on these seed layers are characterized by an im-

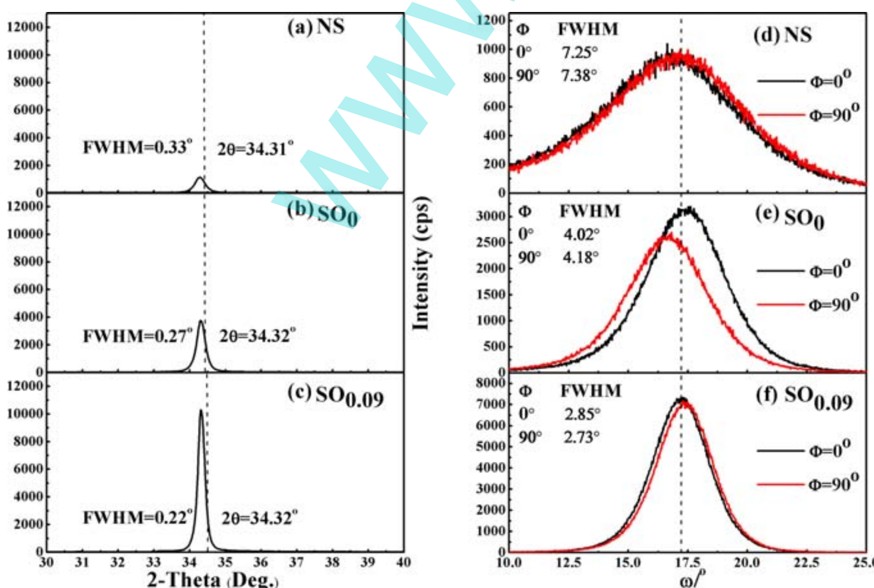

Figure 1 (a–c) XRD patterns of the NS, SO_0 and $SO_{0.09}$ samples in θ–2θ geometry. (d–f) Corresponding rocking curve measurements, the orientation of $\Phi = 0°$ (black) stands for the measurement along a certain direction of the sample, $\Phi = 90°$ (red) stands for a measurement perpendicular to it.

© 2014 WILEY-VCH Verlag GmbH & Co. KGaA, Weinheim

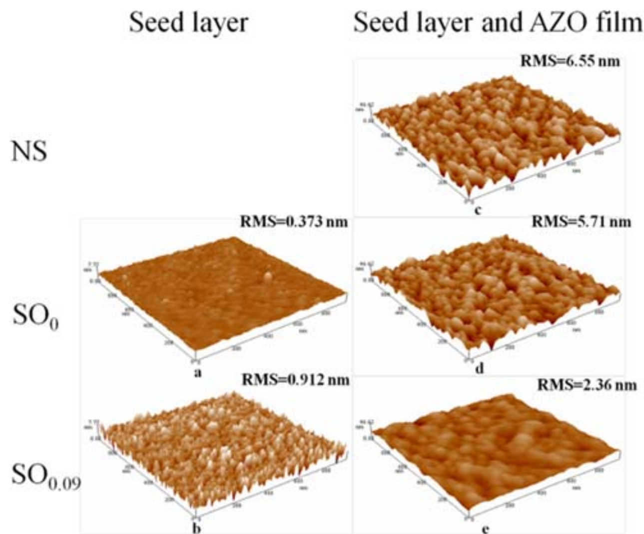

Figure 2 Surface morphologies and RMS roughness of the initial seed layers and the AZO ultra-thin film.

proved orientational order, as the peak position of each sample detected in orientation 0° and 90° becomes closer. The decreased FWHM of these peaks show an improved quality of the out-of-plane texture of AZO thin films. These are due to the improved orientational order of the crystallite *c*-axis along the substrate normal [18], giving rise to a better nucleation regime of the initial thin film growth on the following ultra-thin film growth stages [15].

The surface morphologies and root-mean-square (RMS) roughness of the initial seed layers and the AZO ultra-thin films are displayed in Fig. 2(a–e). It can be seen that the RMS roughness of the seed layers increases from 0.373 nm to 0.912 nm with the ratio of O_2/Ar changed from 0 to 0.09. This means that the (002) orientational order of the initial seed layer is improved. In addition, the AZO ultra-thin films show a significantly reduced RMS roughness from 6.55 nm to 2.36 nm and more obtuse hillcoks, as reported by Miyata [27]. These are attributed to the excellent (002) preferred orientation of the seed layer, which can improve the *c*-axis texture of the following AZO ultra-thin film aligned to the growth direction, and the defects in grain boundary are reduced. The grain size of the AZO ultra-thin films increases from 25 nm to 45 nm estimated according to the AFM graphs (Fig. 2(c–e)), consistent with the results of XRD measurements. Hence, the structural evolution of the following AZO ultra-thin film is governed by the improved structure of the nucleation layer.

3.2 Electrical properties Table 1 shows the electrical properties of the NS, SO_0 and $SO_{0.09}$ samples. When the oxygen-controlled homo-seed layer was employed, the AZO ultra-thin films showed a decreased resistivity from 8.4×10^{-4} Ω cm to 4.2×10^{-4} Ω cm, and the corresponding carrier concentration and mobility increased from 4.2×10^{20} cm^{-3} to 5.2×10^{20} cm^{-3} and 17.7 cm^2 V^{-1} s^{-1} to 28.8 cm^2 V^{-1} s^{-1}, respectively. For the $SO_{0.09}$ sample, the lowest resistivity of 4.2×10^{-4} Ω cm, the highest carrier concentration of 5.2×10^{20} cm^{-3} and the highest mobility of 28.8 cm^2 V^{-1} s^{-1} can be achieved at 200 °C. These are in the same range as the best electrical properties reported by Ellmer et al. [30], considering that this group used magnetron sputtering with excitation frequencies of 27.12 MHz. This highly crystalline homogeneous AZO seed layer with perfect (002) orientational order contributes to the improved (002) orientational order of the following AZO ultra-thin film. This kind of AZO ultra-thin film exhibits less defects [18], less grain boundary scattering [14] and excellent (002) orientation [11], contributing towards the improvement of electrical transport. Interestingly, the carrier concentration of the films with oxygen-controlled homo-seed layer increased, which was different from the carrier concentration decrease reported in literature [31, 32, 25]. This may be attributed to the promoted crystalline quality of AZO films by the initial oxygen-controlled homo-seed layer, reducing the sum of electron traps. Furthermore, the decrease of the aforementioned RMS roughness also contributes towards the improvement of the conductivity of AZO ultra-thin films [33].

3.3 Optical properties The transmittance spectra of the NS, SO_0 and $SO_{0.09}$ samples are shown in Fig. 3. The average transmittance of the NS, SO_0 and $SO_{0.09}$ samples in the wavelength range of 380–780 nm was 85.5%, 86.8% and 85.4%, respectively, including the glass substrate. With the oxygen-controlled homo-seed layer, the transmittance of the AZO films in the infrared range showed a drastic decrease. This decrease is caused by the increase in carrier concentration, which enhances the plasma frequency [25]. When this homo-seed layer was introduced, the ultraviolet absorption edges were blue-shifted. This is attributed to the increased carrier concentration, which can be explained by the Moss–Burstein effect [34]. As seen in Fig. 3, the $SO_{0.09}$ sample indicated the highest carrier concentration and the largest band gap, consistent with the results of Hall measurements.

Table 1 Electrical properties of the NS, SO_0 and $SO_{0.09}$ samples.

sample label	thickness (nm)	R_s (Ω/sq)	resistivity (10^{-4} Ω cm)	carrier concentration (10^{20} cm^{-3})	mobility (cm^2 V^{-1} s^{-1})
NS	169	49.6	8.4	4.2	17.7
SO_0	182	42.0	7.7	4.2	19.3
$SO_{0.09}$	191	21.8	4.2	5.2	28.8

© 2014 WILEY-VCH Verlag GmbH & Co. KGaA, Weinheim

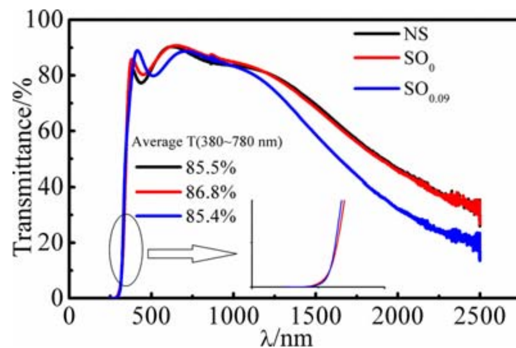

Figure 3 Transmittance spectra (including the glass substrate) of NS, SO_0 and $SO_{0.09}$ samples.

4 Conclusions

In summary, highly transparent and conductive AZO ultra-thin films with oxygen-controlled homo-seed layer were successfully deposited on glass by DC magnetron sputtering home-made AZO ceramic target at the substrate temperature of 200 °C. When the oxygen-controlled homo-seed layer was employed, the resistivity of the AZO ultra-thin films decreased from 8.4×10^{-4} Ω cm to 4.2×10^{-4} Ω cm, and the corresponding carrier concentration and mobility increased from 4.2×10^{20} cm^{-3} to 5.2×10^{20} cm^{-3} and 17.7 cm^2 V^{-1} s^{-1} to 28.8 cm^2 V^{-1} s^{-1}, respectively. The XRD measurements illustrated that the FWHM of the AZO ultra-thin films decreased from 0.33° to 0.22°, corresponding to an increase of the average grain size from 26.8 nm to 43.0 nm with employing the homo-seed layer. The XRD rocking curves revealed that the AZO ultra-thin film grown on the seed layer deposited in atmosphere of O_2/Ar of 0.09 exhibited the most excellent structural order. The transmittance of the AZO ultra-thin film with oxygen-controlled homo-seed layer including glass was 85.4% in the 380–780 nm range. This work reveals that the oxygen-controlled homo-seed layer method is promising for fabricating high-quality AZO ultra-thin films as transparent electrode in FPDs.

Acknowledgements Financial support from the Ningbo Innovative Research Team Program (2009B21005, 2011B82005), NSFC (2097510, 21205127), Ningbo Natural Science Foundation (Grant no. 2011A610009, Grant no. 201201A6105009) and Zhejiang Provincial Natural Science Foundation of China (Grant no. Y4110463, Grant no. LY12E02009) is acknowledged.

References

[1] D. S. Ginley and C. Bright, MRS Bull. **25**, 15 (2000).
[2] H. Hosono, H. Ohta, M. Orita, K. Ueda, and M. Hirano, Vacuum **66**, 419 (2002).
[3] T. Minami and T. Miyata, Thin Solid Films **517**, 1474 (2008).
[4] W. W. Lee, R. P. Dwivedi, C. Hong, H. W. Kim, N. Cho, and C. Lee, J. Mater. Sci. **43**, 1159 (2008).
[5] C. Y. Hsu, T. F. Ko, and Y. M. Huang, J. Eur. Ceram. Soc. **28**, 3065 (2008).
[6] M. L. Addonizio, A. Antonaia, G. Cantele, and C. Privato, Thin Solid Films **349**, 93 (1999).
[7] F. Ruske, T. V. Sittinger, W. Werner, B. Szyszka, K.-U. van Osten, K. Dietrich, and R. Rix, Surf. Coat. Technol. **200**, 236 (2005).
[8] S. H. Lee, T. S. Lee, K. S. Lee, B. Cheong, Y. D. Kim, and W. M. Kim, J. Electroceram. **23**, 468 (2009).
[9] K. Zhu, Y. Yang, T. F. Wei, R. Q. Tan, P. Cui, W. J. Song, and K. L. Choy, Mater. Lett. **106**, 363 (2013).
[10] D. J. Kwak, M. W. Park, and Y. M. Sung, Vacuum **83**, 113 (2009).
[11] T. Yamada, A. Miyake, S. Kishimoto, H. Makino, N. Yamamoto, and T. Yamamoto, Appl. Phys. Lett. **91**, 051915 (2007).
[12] Z. Haibo, D. Guotao, L. Yue, Y. Shikuan, X. Xiaoxia, and C. Weiping, Adv. Funct. Chem. **20**, 561 (2010).
[13] K. Ellmer, Nature Photon. **6**, 809 (2012).
[14] B. Szyszka, W. Dewald, S. K. Gurram, A. Pflug, C. Schulz, M. Siemers, V. Sittinger, and S. Ulrich, Curr. Appl. Phys. **12**, S2 (2012).
[15] D. Köhl, M. Luysberg, and M. Wutting, J. Phys. D, Appl. Phys. **43**, 205301 (2010).
[16] M. Birkholz, B. Selle, F. Fenske, and W. Fuhs, Phys. Rev. B **68**, 205414 (2003).
[17] M. Kumar, R. M. Mehra, A. Wakahara, M. Ishida, and A. Yoshida, Thin Solid Films **484**, 174 (2005).
[18] D. Köhl, M. Luysberg, and M. Wutting, Phys. Status Solidi RRL **3**, 236 (2009).
[19] D. Köhl, G. Natarajan, and M. Wutting, J. Phys. D, Appl. Phys. **45**, 245302 (2012).
[20] T. Yamamoto, H. P. Song, and H. Makino, Phys. Status Solidi C **10**, 603 (2013).
[21] T. Terasko, H. Song, H. Makino, S. Shirakata, and T. Yamamoto, Thin Solid Films **528**, 19 (2013).
[22] J. H. Liu, C. H. Lin, C. C. Yang, and I. M. Chan, in: Proceedings of the 37th IEEE Photovoltaic Specialists Conference, Seattle, WA, 2011 (IEEE, New York, 2011), pp. 649–651.
[23] Y. F. Chen, J. S. K. Hong, H. J. Ko, V. Kirshner, H. Venisch, T. Yao, K. Inaba, and Y. Segawa, Appl. Phys. Lett. **78**, 3352 (2001).
[24] N. Itagaki, K. Kuwahara, K. Nakahara, D. Yamashita, G. Uchida, K. Koga, and M. Shiratani, Appl. Phys. Express **4**, 011101 (2011).
[25] D. Y. Wan, F. Q. Huang, Y. Y. Wang, X. L. Mou, and F. F. Xu, ACS Appl. Mater. Interfaces **2**, 2147 (2010).
[26] Q. K. Li, J. B. Wang, B. Li, X. L. Zhong, F. Wang, and C. B. Tan, Appl. Sur. Sci. **283**, 623 (2013).
[27] J. I. Nomoto, J. I. Oda, T. Miyata, and T. Minami, Thin Solid Films **519**, 1587 (2010).
[28] Y. L. Zhang, Y. Yang, J. H. Zhao, R. Q. Tan, P. Cui, and W. J. Song, J. Sol–Gel Sci. Technol. **51**, 198 (2009).
[29] N. Fujimura, T. Nishihara, S. Goto, J. F. Xu, and T. Ito, J. Cryst. Growth **130**, 269 (1993).
[30] A. Bikowski, T. Welzel, and K. Ellmer, Appl. Phys. Lett. **102**, 242106 (2013).
[31] D. W. Kang, S. H. Kuk, K. S. Ji, S. W. Ahn, and M. K. Han, Jpn. J. Appl. Phys. **49**, 031101 (2010).
[32] O. Kluth, G. Schöpe, B. Rech, R. Menner, M. Oertel, K. Orgassa, and H. W. Schock, Thin Solid Films **502**, 311 (2006).
[33] S. J. Tark, Y. W. Ok, M. G. Kang, H. J. Lim, W. M. Kim, and D. Kim, J. Electroceram. **23**, 548 (2009).
[34] E. Burstein, Phys. Rev. **93**, 632 (1954).

www.spm.com.cn

© 2014 WILEY-VCH Verlag GmbH & Co. KGaA, Weinheim